

## Experimental studies of defect dynamics and interaction in electrohydrodynamic convection

Steffen Rasenat and Victor Steinberg

*Department of Nuclear Physics, Weizmann Institute of Science, Rehovot, 76100, Israel*

Ingo Rehberg

*Physikalisches Institut der Universität Bayreuth, D-8580 Bayreuth, West Germany*

(Received 1 March 1990)

A report about experimental studies of the dynamics and interaction of topological defects in the roll structure of electrohydrodynamic convection in nematic liquid crystals is given. It is found that the motion of defects of opposite topological charges towards annihilation has two stages. At large distances they move with a constant velocity that depends mainly linearly on the wave-number mismatch. At a later stage, when the defects come closer, they are accelerated due to attraction. In order to compare these results quantitatively with available theories that are based on the Ginzburg-Landau equation, all coefficients of this equation are measured.

### I. INTRODUCTION

It is well established that the transition to chaotic behavior in spatially extended systems occurs through a loss of spatial coherency together with the onset of temporal complexity. In isotropic pattern-forming systems, for which Rayleigh-Bénard convection is a prominent example, in large-aspect-ratio containers "textured" structures with many different types of defects are the general rule.<sup>1</sup> Both the rotational invariance in a horizontal plane and the lateral boundaries are responsible for this complexity. The texture that appears near the threshold either relaxes toward the stationary state or leads to weak turbulence (time-dependent nonrelaxational behavior).

In both cases spatiotemporal dynamics of the texture is closely related to the dynamics of the defects. For an ideal pattern structure the system loses the structure coherency just through the nucleation of topological defects (dislocations) while a control parameter is increased.<sup>2-4</sup> In anisotropic pattern-forming systems, for which electrohydrodynamic convection (EHC) is a canonical example, an ideal pattern structure can be achieved near the threshold due to an appropriate sample preparation.<sup>5</sup>

Thus in both isotropic and anisotropic cases the complex regime called "spatiotemporal turbulence," or "weak turbulence," is typically accompanied by the appearance of defects. Their dynamics defines the specific features of the state. In order to understand the complex dynamics of the weak turbulence, it is natural to study first the dynamics and interaction of topological defects. Moreover, for the reasons presented below, EHC is considered as an appropriate system to study the problem.

There have been several experimental studies of the defect motion in recent years. The most extensive semi-quantitative studies were conducted on the climbing motion of an isolated dislocation induced in an otherwise ideal roll structure of Rayleigh-Bénard convection.<sup>4</sup> It was shown<sup>4</sup> that the dislocation motion along the roll

axis (climb) provides an effective wave-vector selection mechanism. However, the experiments were mostly performed at high values of the control parameter  $R$  (here  $R$  is the Rayleigh number), where perturbative theories are expected to break down. At small values of the control parameter where the theoretical predictions are valid, a dislocation does not move smoothly but shows small abrupt variations in its position.<sup>4</sup> It is not clear what the reasons for such discrepancies are. One of the possible explanations could be the method of stabilization of initially ideal roll structures by sidewall heating.<sup>4</sup> Nevertheless, this experiment demonstrated that the dislocation climb occurred with a uniform velocity, at least in some range of the control parameter which was a fundamental result of theoretical works.

Another important and earlier experimental study of the velocity of motion of a row of dislocations<sup>6</sup> gives valuable information about the Prandtl number dependence. The latter experiment<sup>6</sup> initiated theoretical studies of the dislocation motion.<sup>7-9</sup> The main result is the relation between the climbing velocity and the deviation of the wave number  $k$  of the structure from the critical one  $k_c$  for small enough values of the control parameter  $R$ . It was also shown that the gliding motion of a dislocation (perpendicular to the roll axis) does not occur in the potential case.<sup>8,9</sup>

The role of the vertical vorticity in defect dynamics was studied in Refs. 9 and 10. It was emphasized that since the vertical vorticity always appears together with dislocations it should be taken into account explicitly in the modified amplitude equation.<sup>11</sup> As was shown,<sup>10</sup> this is a way to incorporate nonvariational terms into the amplitude equation and to study their effects on dislocation motion. However, later studies showed that the vertical vorticity does not have a strong effect on the defect dynamics.<sup>9</sup> Another result in the same paper<sup>9</sup> is that gliding should show pinning to an underlying short scale structure. A study of defects in waves using topological arguments and numerical simulations is given in Ref. 12.

More intensive studies of the defect dynamics were conducted in anisotropic flows. First, in a series of several papers,<sup>13–16</sup> a theoretical phenomenological model based on the phase diffusion equation was used to describe the defect dynamics and the strain field around it for the shear-flow instability.<sup>14</sup> An analogy between the elasticity of smectic layers and the roll structure was developed to describe the deformation field around an individual defect. It was suggested that, in the case of a static defect, a characteristic length of the order-parameter field exists. This characteristic length, which corresponds to the penetration length in smectic liquid crystals, can be introduced if one takes into account the curvature elasticity of the roll structure. In the case of the shear-flow instability, this length tends to be smaller than the cell depth  $d$ .<sup>15,16</sup>

Recently, several experimental studies on defects were performed on EHC in nematic liquid crystals. A study of the statistics of defects in traveling waves is given in Ref. 17. A description of the shape of dislocations was given in Ref. 5. The dynamics and the interaction of defects were studied recently.<sup>18–21</sup> Defect dynamics during the pattern formation process near the threshold for Williams rolls (WR, sometimes also called Williams domains) together with the statistics and the frequency spectrum of WR near the threshold of a defect nucleation were studied quantitatively in a relatively thick cell (100  $\mu\text{m}$ ).<sup>18–20</sup> In Ref. 18, the dynamic of single defect was measured during the evolution process of the pattern which makes the theoretical description difficult. A recently published experiment<sup>21</sup> with well-controlled initial conditions was conducted in a cell with specially prepared interdigital electrodes. The results obtained show a contradiction to the theory, probably because of the electrode design. Another interesting issue is the nature of the transition from very well-ordered WR to a defect-mediated spatiotemporal disordered structure.<sup>20,22</sup> It was claimed in Ref. 20 that the transition from WR to fluctuating WR (this is a defect-affected WR state where defects never disappear) is a hysteretic first-order phase transition while in Ref. 22 the authors claim that it is an activation energy process; i.e., there is no well-defined transition.

During the past two years two theories of the defect nucleation, dynamics, and interaction in an anisotropic flow based on different ideas were suggested. The first one<sup>23,24</sup> is based on the amplitude equation and assumes that this equation can describe the structure and dynamics of dislocations in anisotropic pattern-forming systems. The appropriate solution for the dislocation core and the far phase field which bears the important topological properties of a defect, was obtained from the amplitude equation. The equation was derived from conservation-law equations and is similar to the Ginzburg-Pitaevskii equation for superfluid helium. A defect is an analog to a quantum vortex in the latter case. In contrast to the isotropic case both glide and climb are possible in EHC due to this theory. Another theory<sup>25</sup> (the ideas and results of this theory are also explained in Ref. 3; in Ref. 25 a more detailed derivation of this theory is given) takes a different approach: The authors of Ref. 25 claim that since the amplitude equation describes just long-

wavelength perturbations it cannot describe correctly a singularity of the amplitude field on the short scale. The presence of defects suggests an introduction of an additional degree of freedom that may be presented by a gauge field. This phenomenological theory based on a gauge symmetry consideration introduces a new characteristic length in the system, in addition to the coherence length.

This paper deals with the dynamic and interaction of defects in a stationary roll structure. The main characteristics of the experiment are as follows.

(i) The sample preparation leads to well-ordered structures without any structural defects on the scale of the sample (about 2000 rolls). The sample is stable on the level of resolution for a period of several weeks.

(ii) It was possible to change the wave number of the roll structure in a well-controlled way by using the dependence of the critical wave number on the frequency of the driving ac voltage. Thus the defect dynamics and interaction as a function of the control parameter and the wavelength could be studied.

(iii) A digital filtering technique (complex demodulation) allows pinpointing the defect core with a spatial resolution in the order of 1  $\mu\text{m}$  (Fig. 2).

For quantitative studies of the defect dynamics and their interaction and the comparison of the results with available theories one needs to measure all parameters which appear in the theoretical models. This was done for Rayleigh-Bénard convection,<sup>26</sup> which is a canonical system for quantitative studies of pattern formation and dynamics based on the Ginzburg-Landau (GL) equation, more than ten years ago. The experimental determination of the coefficients of the GL equation for an anisotropic system is presented in this paper. The values of the coefficients are in a reasonable agreement with theoretical calculations.<sup>27</sup> A short report on the dynamics and interaction of topological defects in EHC was published elsewhere.<sup>3</sup>

The paper is organized as follows. We describe our sample preparation procedure and experimental techniques in Sec. II. The measurement of the coefficients of the GL equation is described in Sec. III, and experimental results on the defect dynamics and interaction are given in Sec. IV. A discussion of the results and conclusions are presented in Sec. V.

## II. EHC IN NEMATIC LIQUID CRYSTALS, SAMPLE PREPARATION, AND EXPERIMENTAL TECHNIQUES

When an ac voltage with a low frequency is applied across a thin layer of a nematic liquid crystal having negative dielectric anisotropy  $\epsilon_a$ , sufficient ionic conductivity  $\sigma$ , and uniform orientation of the director  $\mathbf{n}$  in the layer an instability from the uniform electroconductive basic state to a stationary periodic pattern of convecting rolls (WR) occurs at a threshold value of the voltage amplitude.<sup>27</sup> In the low-frequency conductive regime the periodic pattern is related to an almost static periodic distortion of the direction field.<sup>27</sup> When the frequency  $f$  of the applied ac field is varied the critical voltage  $V_c(f)$  and

the critical wavelength of the structure  $k_c(f)$  change. The conductive regime exists up to the cutoff frequency  $f_c$  at which the nature of the instability changes.<sup>27</sup> For a simplified theory this cutoff frequency is approximately

$$f_c = \frac{1}{2\pi\epsilon_0} \left[ \frac{\sigma_{\parallel}}{\epsilon_{\perp}} \left( \frac{\alpha_2 \sigma_a}{\eta_1 \epsilon_a} - \frac{\alpha_2 \sigma_{\parallel}}{\eta_1 \epsilon_{\parallel}} - \frac{\sigma_{\perp}}{\epsilon_{\perp}} \right) \right]^{1/2}, \quad (1)$$

where  $\sigma_{\parallel}$  and  $\sigma_{\perp}$  are the electrical conductivity in directions parallel and perpendicular to the director  $n$ ;  $\sigma_a = \sigma_{\parallel} - \sigma_{\perp}$  is the conductivity anisotropy;  $\epsilon_a = \epsilon_{\parallel} - \epsilon_{\perp}$  is the dielectric anisotropy which is negative for the nematic liquid crystal that was used [4-methoxybenzylidene-4'-*n*-butylaniline (MBBA)];  $\alpha_2$  and  $\eta_1$  are the viscosity coefficients; and  $\epsilon_0$  is the dielectric constant of the vacuum. Both  $V_c$  and  $k_c$  diverge at  $f_c$  and the conductive regime ceases to exist above  $f_c$ , where the nature of the instability changes.

The weakly nonlinear behavior of EHC in the conductive regime is reminiscent of the Rayleigh-Bénard convection. However, the former system has a number of advantages which makes it particularly suitable for studies of spatiotemporal turbulence in large aspect ratio systems. These specific advantages are (i) the possibility to use a very thin layer of a nematic liquid crystal in EHC leads to very short relaxation times, which is usually a strong limitation to study large aspect ratio systems; (ii) small thickness and an experimental technique to produce the pattern oriented with respect to the preferred axis give the opportunity to prepare almost ideal samples with a large aspect ratio in one or two directions; (iii) easily accessible control parameters such as the amplitude and the frequency of the applied ac voltage make the system very convenient for experimental studies.

The mechanism of the stationary instability in the conductive regime is well understood,<sup>28</sup> and all parameters necessary to describe linear and weakly nonlinear dynamics were recently calculated in detail.<sup>27</sup>

#### A. Sample preparation and apparatus

The experiments were done in a thin layer of the nematic liquid crystal MBBA confined between transparent electrodes. The horizontal dimensions of the cell are  $30 \times 7 \text{ mm}^2$  and the depth of the cell is  $15 \mu\text{m}$ , so that one gets about 2000 convection rolls. In order to achieve a uniform unidirectional alignment of the molecules in the whole sample the electrodes were covered by a polymer and subsequently rubbed unidirectionally. This technique together with the filling procedure leads to a unique orientation of the convection rolls above the onset. The cell was sealed completely with epoxy. The temperature of the water bath was stabilized to  $21 \pm 0.01^\circ\text{C}$ . Under these conditions the rate of deterioration of MBBA was negligible on the time scale of many days so that the critical voltage of the convection onset  $V_c$  was reproducible and stable within 2% during 30 days.

The experimental results on the critical voltage  $V_c$  and the critical wave number  $k_c$  of the Williams rolls as a function of the reduced external frequency  $f/f_c$  are

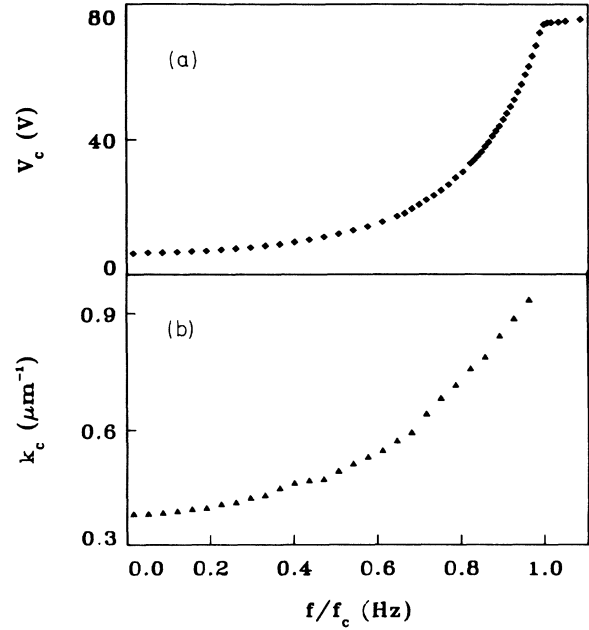


FIG. 1. (a) The critical voltage  $V_c$  and (b) the critical wave number  $k_c$  are shown as a function of the external frequency  $f/f_c$  ( $f_c = 570 \text{ Hz}$ ).

shown in Fig. 1. The cutoff frequency  $f_c$  of the sample is at  $570 \text{ Hz}$ . Most of the experiments were done at  $f = 114 \text{ Hz}$  or  $f/f_c = 0.2$ , i.e., far away from the cutoff frequency. We use further on the reduced values of the control parameter  $\epsilon = (V^2 - V_c^2)/V_c^2$  and  $f/f_c$ . The WR are observable under a microscope with polarized light due to the anisotropy of the refraction index of the nematic liquid crystals.<sup>29</sup> In Fig. 2(a) a shadowgraph image of the convection rolls is shown with five gray scales taken with a charge-coupled-device (CCD) camera and digitized by a frame grabber with a spatial resolution of  $512 \times 512$  pixels and an 8-bit gray scale resolution.

The wave number of the pattern was obtained by performing a fast Fourier transform (FFT) on lines in the  $x$  direction (perpendicular to the rolls) and interpolation in the discrete values of the power spectrum. For pictures with one or two defects, the wave number on the side of

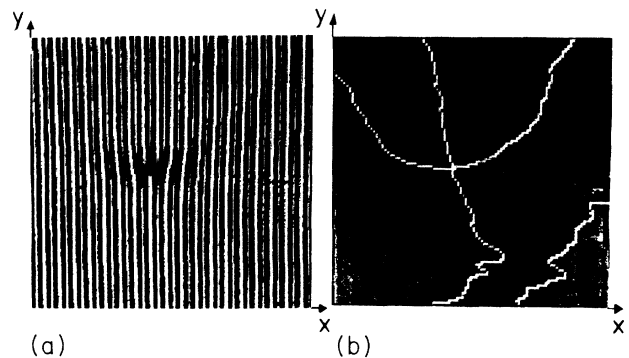


FIG. 2. (a) A shadowgraph image of a single defect in Williams rolls, and (b) the corresponding field of the absolute value of the amplitude and two lines corresponding to  $\text{Re}(A) = 0$  and  $\text{Im}(A) = 0$ .

the defect(s) with one period less was taken. It was not possible to measure a wave number in the  $y$  direction (i.e., the tilt of the rolls). Therefore no quantitative studies of the glide motion of defects could be made. The wave number  $k$  always means  $k_x$  in this paper.

### B. Digital filtering of pattern images

In order to study quantitatively the defect dynamics and also to get the correlation lengths of the amplitude field we used digital filtering of the pattern images. The roll pattern in the 2D space  $(x,y)$  can be presented by

$$\phi(x,y) = A(x,y)e^{ikx} + \text{c.c.}, \quad (2)$$

where  $k$  is the wave number of the roll structure and  $A(x,y)$  is the complex amplitude field which describes slow variations. At the defect core both  $\text{Re}(A)$  and  $\text{Im}(A)$  are vanishing. Far from the defect  $A(x,y)$  mostly describes slow variations of the phase field. However, near the core it describes also variations in the amplitude field. In order to remove fast variations with the wave number  $k$  we used a 2D FFT. Because there is only a periodicity of the pattern in the  $x$  direction, it is also possible to demodulate the pattern by using only 1D FFT's performed on the 512 lines of the picture. The FFT gives the Fourier transformation of the complex and the complex-conjugate (c.c.) part of  $\phi$  as complex and complex-conjugate numbers. By taking only the complex part of the spectrum (the complex-conjugate part is set equal to zero), isolating the peak at  $k$ , and shifting it to the origin of the Fourier space the periodicity with the wave number  $k$  is taken out of the Fourier spectrum. In the sideband of  $k$  is the information about the complex amplitude  $A(x,y)$  [because of  $A(x,y)e^{ikx} = \sum_m A_m(y)e^{iK_m x} e^{ikx} = \sum_m A_m(y)e^{i(k+K_m)x}$ ]. In our spectrum we have not only the wave number  $k$  but also the higher harmonics ( $2k, 3k, \dots$ ), which have to be filtered out. After this procedure we perform the FFT back to the real space and obtain the complex amplitude field  $A(x,y)$  without rapid spatial variations, i.e., without the underlying pattern. The minimum of the magnitude of  $A$  is the location of the defect core. We tested this procedure for a model of a 1D defect  $\Phi(x) = \tanh[(x-z)/\xi] \sin(kx)$ . The location of the core is at  $x=z$ . For 20 or more periods of the sine (a grid of 512 points for  $x$  was used) the error for the location of the core we found was less than 0.01% of the wavelength of the sine.

The absolute value of the amplitude field  $A(x,y)$  which corresponds to the shadowgraph image of the roll pattern in Fig. 2(a) is shown in Fig. 2(b). At the location of the defect a black elliptical spot can be seen. The white lines show  $\text{Re}(A)=0$  and  $\text{Im}(A)=0$ , and their intersection defines the location of the defect core. This technique allows us to pinpoint the core with a spatial resolution of the order of  $\pm 1 \mu\text{m}$  (the main limitation of the resolution is the appearance of higher harmonics in the spectrum). Thus this method gives us a possibility to study quantitatively the defect dynamics [see e.g., Figs. 3(a) and 3(b)].

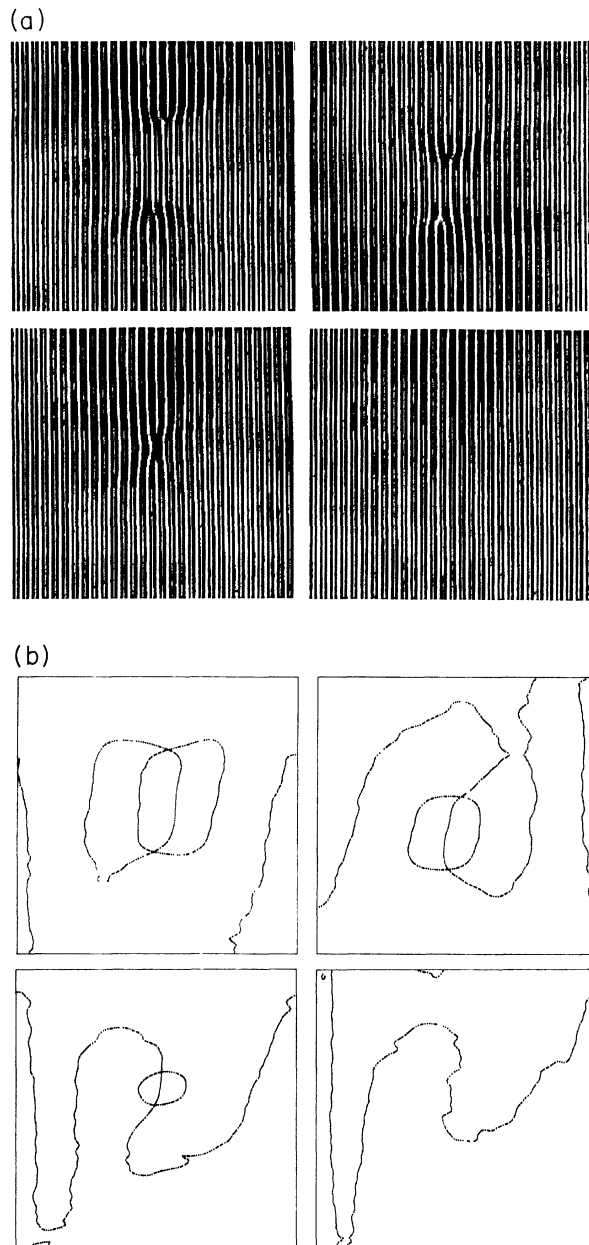


FIG. 3. (a) Dynamics of defect annihilation presented in four pictures in time, and (b) the same process but presented in the phase field plane after the digital filtering.

### III. EXPERIMENTAL DETERMINATION OF THE COEFFICIENTS OF THE GINZBURG-LANDAU EQUATION

To study quantitatively the defect dynamics and make a comparison with the theoretical results based on the GL equation one needs first to find experimentally the characteristic time, length, and the nonlinear coefficient which appear in the GL equation. Together with the critical voltage  $V_c(f/f_c)$ , the critical wave number  $k_c(f/f_c)$ , and the optimal wave number  $k_f(\epsilon)$  ( $k_f$  is the wave number where the velocity of a single defect in the pattern is equal to zero) of the pattern, one gets a full set

of the parameters which are necessary to describe the linear and nonlinear dynamics of the WR close to the onset.

The amplitude equation for the roll pattern in an anisotropic system like EHC can be written in the following form:<sup>27</sup>

$$\tau_0 \frac{\partial}{\partial t} A = \varepsilon A + \left[ \xi_{\parallel}^2 \frac{\partial^2}{\partial x^2} + \xi_{\perp}^2 \frac{\partial^2}{\partial y^2} \right] A - g |A|^2 A, \quad (3)$$

where  $\tau_0$  is the relaxation time,  $\xi_{\parallel}^0$  and  $\xi_{\perp}^0$  are the longitudinal and transversal coherence lengths, respectively,  $g$  is the nonlinear coupling coefficient, and  $\varepsilon$  is the control parameter of the problem. All parameters are functions of the external frequency  $f/f_c$ . By definition the relaxation time  $\tau_0$  is equal to  $(\partial\sigma/\partial\varepsilon)^{-1}$  at  $k_x = k_c$  and  $k_y = 0$  where  $\sigma$  is the growth rate and  $k_x$  and  $k_y$  are the wave numbers perpendicular to and along the rolls. The coherence lengths  $\xi_{\parallel}^0$  and  $\xi_{\perp}^0$  are defined from the curvatures of the neutral surface at  $\varepsilon = 0$  and  $k_x = k_c, k_y = 0$ . These definitions will be used to find experimental values of these parameters.

To get the value of  $\tau_0$  the central region of the cell with about 40 rolls was studied. The spatial variations of the amplitude in this region is negligibly small, because it is located far away from the lateral boundaries. In that case the amplitude equation describes just the temporal behavior of the amplitude. The experiment was conducted by jumping several times from a value of the control parameter above the threshold value to values below the threshold value; from a fixed  $\varepsilon_c > 0$  to different  $\varepsilon < 0$ . An example of the time dependence of the averaged rms intensity of the shadowgraph picture for one jump is shown in Fig. 4. Starting from a small  $\varepsilon_c$  (typically  $\varepsilon_c \leq 0.02$ ) mainly the linear part of the GL equation describes the decay of the pattern and we get the exponential decay  $A = A_0 e^{\sigma t}$  with  $\sigma = \varepsilon/\tau_0$  and  $\varepsilon < 0$ . The nonlinearities of the shadowgraph method can be avoided by taking the pictures far enough from the image plane where the caustic appears.<sup>29</sup> The solid line in Fig. 4 is the exponential fit to the experimental data.

In Fig. 5 the  $\varepsilon$  dependence of the decay rate  $\sigma$  for the external frequency  $f/f_c = 0.2$  is presented. The slope of

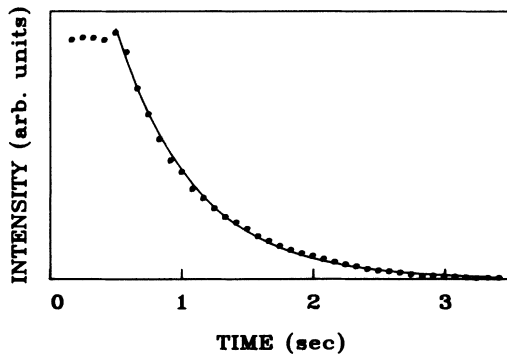


FIG. 4. Intensity of the optical signal as a function of time. The solid line is an exponential fit to the decay. The jump was from  $\varepsilon = 0.02$  to  $\varepsilon = -0.035$  at  $t = 0.5$  sec.  $f/f_c = 0.2$ .

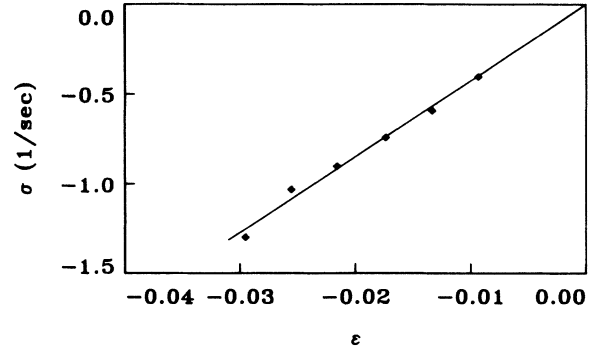


FIG. 5. Linear decay rate  $\sigma$  as a function of the control parameter  $\varepsilon$ . The solid line is a linear fit to the data. The slope  $(1/\tau_0)$  defines  $\tau_0 = 0.048 \pm 0.003$  sec.  $f/f_c = 0.2$ .

the fitted straight line  $(1/\tau_0)$  gives the value of the characteristic time with  $\tau_0 = 0.048 \pm 0.003$  sec at 21 °C. The frequency dependence of  $\tau_0$  at two temperatures of the sample (21 °C and 25 °C) is presented in Fig. 6. Good agreement with the theory<sup>27</sup> is evident.

The values of the coherence lengths were determined by two different techniques. The first method was based on the fact that the spatial variation of the amplitude in the defect core is scaled by the coherence length.<sup>30</sup> Using the digital filtering technique described before we obtained the amplitude variation in the defect core which is presented in Fig. 7 by two cuts through the core of the defect parallel and perpendicular to the underlying pattern. The amplitude field near the defect core is described by the right-hand side of Eq. (3) with  $A = 0$  at the core center and  $A = A_0$  at infinity for the boundary conditions. The numerical solution of the 2D problem is fairly close to the well-known solution of the 1D problem in the  $x$  and  $y$  directions. We can therefore use the approximate solution

$$A(x=0, y) = A_0 \tanh(y/\xi_{\perp}), \quad (4a)$$

$$A(x, y=0) = A_0 \tanh(x/\xi_{\parallel}), \quad (4b)$$

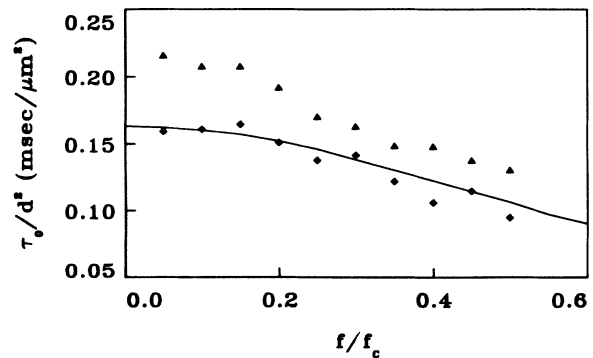


FIG. 6. The scaled characteristic time  $\tau_0/d^2$  as a function of the reduced frequency  $f/f_c$ . The solid line is the theoretical calculation from Ref. 27 (at 25 °C). Triangles present the measurement at 21 °C, diamonds at 25 °C. The error for  $\tau_0$  is less than 10%.

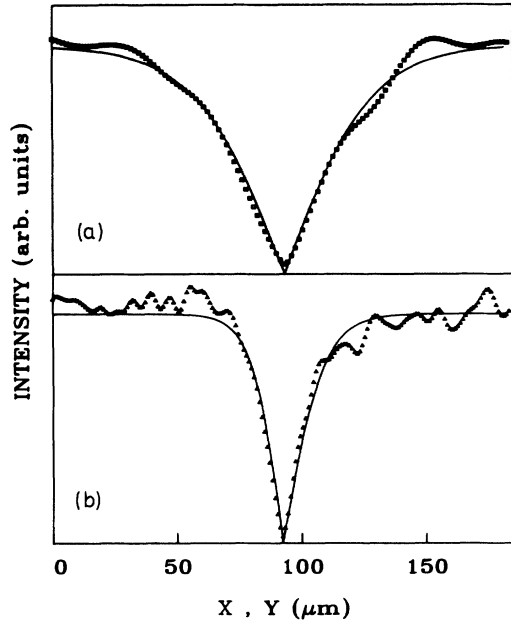


FIG. 7. Cuts of the amplitude field through the defect core in two perpendicular directions: (a) cut in  $x$  direction; (b) cut in  $y$  direction. The solid lines are the fit to the data (see text).  $\varepsilon=0.02$ .

with  $\xi_{\perp} = \xi_{\perp}^0 (2/\varepsilon)^{1/2}$ , and  $\xi_{\parallel} = \xi_{\parallel}^0 (2/\varepsilon)^{1/2}$ , to get the values of the coherence lengths from the fit of the profiles given in Fig. 7. Both coherence lengths as a function of the control parameter at  $f/f_c=0.2$  are presented in Fig. 8. The 2D solution for the amplitude will drop steeper at the defect core, so we will get an upper limit for the coherence lengths with the fit of the 1D solution. We compared the shape of the amplitude at the defect core of the 2D solution taken from Ref. 23 with the 1D solution. The drop near the defect core, which determines mainly

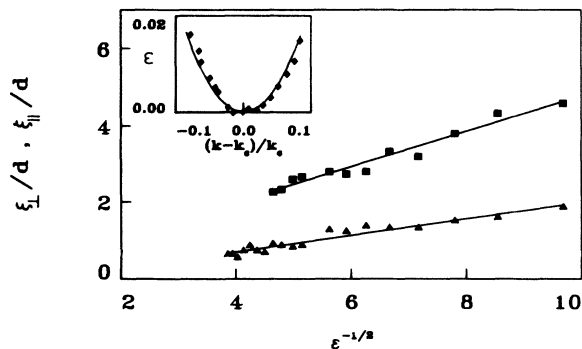


FIG. 8. Longitudinal  $\xi_{\parallel}$  (triangles) and transversal  $\xi_{\perp}$  (squares) coherence lengths as a function of the control parameter  $\varepsilon^{-1/2}$ . Solid lines are a linear fit to the data from which the characteristic lengths in the system  $\xi_{\parallel}^0$  and  $\xi_{\perp}^0$  are defined. Inset: measured neutral curve for the onset of convection. The solid line is the fit of  $\varepsilon = \xi_{\parallel}^0{}^2 (k - k_c)^2 / k_c^2$  to it to get  $\xi_{\parallel}^0$ . From the fit:  $\xi_{\parallel}^0/d = 0.29$ .  $f/f_c = 0.3$

the coherence lengths, is about 25% steeper for the 2D solution. That means that the coherence lengths are smaller at this amount than those we get from the fit of the 1D solution [Eq. (4)]. The results for the coherence lengths based on the 2D solution at  $f/f_c=0.2$  are  $\xi_{\parallel}^0/d = 0.26 \pm 0.05$ ,  $\xi_{\perp}^0/d = 0.12 \pm 0.03$ ,  $\xi_{\parallel}^0/\xi_{\perp}^0 = 2.2 \pm 0.4$ , while the theoretical values<sup>27</sup> at this frequency are  $\xi_{\parallel}^0/d = 0.28$ ,  $\xi_{\perp}^0/d = 0.10$ ,  $\xi_{\parallel}^0/\xi_{\perp}^0 = 2.8$ .

To check the reliability of this method we also used another more common technique to obtain the coherence length from the curvature of the neutral curve at  $k = k_c$ . This was done in a different sample (MBBA,  $d = 12 \mu\text{m}$ ) at a different frequency  $f/f_c = 0.3$ . It is only possible to get  $\xi_{\parallel}^0$  with this method:

$$\xi_{\parallel}^0/d = \begin{cases} 0.24 \pm 0.05 \\ 0.29 \pm 0.03 \end{cases}$$

from the fit to the core profile and the neutral curve (Fig. 8, inset), respectively. Longitudinal and transversal coherence lengths as a function of the reduced frequency based on the 1D solution (open symbols) and based on the 2D solution<sup>23</sup> (closed symbols) are presented in Fig. 9. Good agreement between the theory<sup>27</sup> and the experimental data analyzed on the basis of the full 2D solution of the defect core is demonstrated in Fig. 9.

To have the complete set of coefficients of the GL equation we also measured the amplitude of the director distortion angle  $\theta_0$  as a function of the reduced frequency using the method from Ref. 29. This gives us the non-linear coefficient of the GL equation  $g = \theta_0^{-2}$ , and in spite of the scatter the agreement with the theory<sup>27</sup> is reasonable (Fig. 10). This value of  $g$  is valid for the GL equation, when the amplitude  $A(x,y)$  is chosen to be the director distortion angle in degrees.

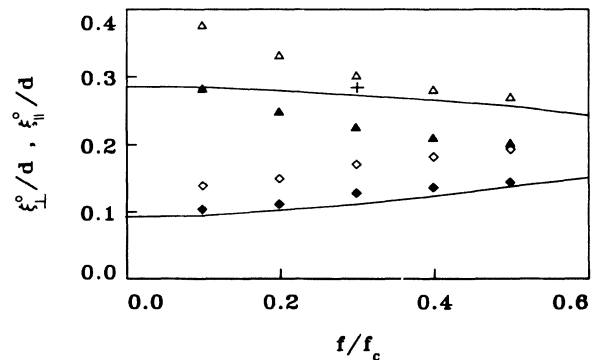


FIG. 9. Longitudinal and transversal characteristic lengths of the systems as a function of the reduced frequency  $f/f_c$ . Open symbols present the data analyzed by using the 1D solution for the defect core, closed symbols present the data analyzed with the 2D solution, triangles correspond to the data for  $\xi_{\parallel}^0$ , diamonds for  $\xi_{\perp}^0$  (the error for this value is less than 20%). The solid curves are the theoretical calculations (Ref. 27) for these lengths, respectively. The cross is the value for  $\xi_{\parallel}^0$  taken from the neutral curve (Fig. 8, inset).

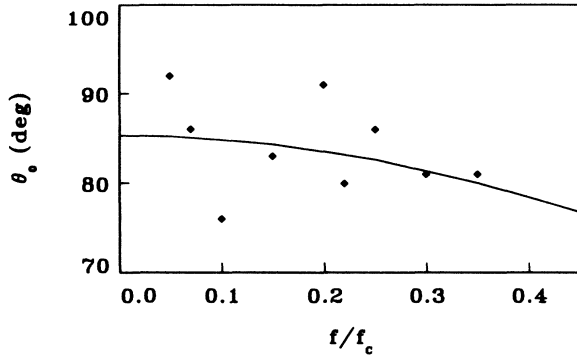


FIG. 10. The director distortion angle  $\theta_0$  as a function of the reduced frequency  $f/f_c$ . The solid line presents the calculation from Ref. 27.

In order to study the defect dynamics one needs also to know the optimal wave number  $k_f(\epsilon, f/f_c)$ . The theory<sup>23,24</sup> predicts that the defect motion serves as a wave-number selection mechanism, and the velocity of an isolated defect depends on the deviation of the wave number of the underlying pattern from  $k_f$ . For  $k = k_f$  the velocity should be zero. We measured the velocity of the defect motion as a function of the wave number at two values of the control parameter  $\epsilon = 0.03$  and  $0.06$ . The results of the measurements at  $\epsilon = 0.06$  are shown in Fig. 11 where the value for  $k_f$  is taken from the intersection of the fitted straight line with the  $k$  axis to  $k_f = 0.3814 \pm 0.002 \mu\text{m}^{-1}$ . At  $\epsilon = 0$  one has  $k_f = k_c$ .  $k_c$  was measured by applying a slightly overcritical voltage ( $\epsilon \cong 10^{-4}$ ) so that the pattern will develop slowly without defects. The result of several runs gives  $k_c = 0.3769 \pm 0.0005 \mu\text{m}^{-1}$ . The values of  $k_f$  and  $k_c$  are shown by triangles in Fig. 11. This gives (assuming a linear dependence)  $k_f = s_f \epsilon + k_c$  with  $s_f = 0.072 \pm 0.016 \mu\text{m}^{-1}$ .

We compared this with the wave number corresponding to the maximal growth rate. As suggested in Ref. 23

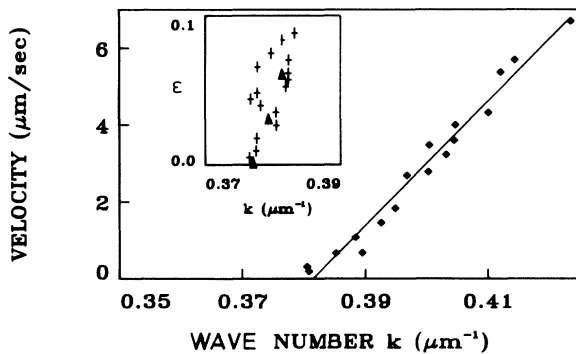


FIG. 11. Constant defect velocity  $u$  as a function of the wave number  $k$  for  $\epsilon = 0.06$ . The intersection of the linear fit (solid line) with  $u = 0$  gives the value of the optimal wave number  $k_f$  (band center). In the inset the optimal wave number  $k_f$  as a function of  $\epsilon$  is shown (triangles) and the wave number corresponding to the maximal growth rate is presented (crosses).

a sudden jump to a supercritical value of the control parameter through the threshold imposes the fastest-growing mode  $k_j(\epsilon)$  while an adiabatic change of  $\epsilon$  favors  $k_c$ . The result of the experiment is presented in the inset of Fig. 11 with crosses. The large scatter is due to the fact that defects often appear together with the pattern after jumping from  $\epsilon < 0$  to  $\epsilon > 0$ , and they slightly change the wave number. For a smaller value  $\epsilon > 0$  fewer defects appear and the corresponding scatter is less. This measurement gives at a frequency of  $f/f_c = 0.2$  (assuming again a linear dependence)  $k_j = s_j \epsilon + k_c$  with  $s_j = 0.059 \pm 0.019 \mu\text{m}^{-1}$ . Within the errors it is possible that the fastest-growing mode  $k_j$  corresponds to the optimal wave number  $k_f$ , but because of the large scatter it is not possible to make a definitive decision.

#### IV. EXPERIMENTAL RESULTS ON DEFECT DYNAMICS

According to the theoretical predictions<sup>23-25</sup> defects in an anisotropic flow climb or glide [Figs. 12(a) and 12(b)] depending on whether the underlying structure has a wave number  $k$  different from the optimal one  $k_f$  (in the case of climbing) or the rolls are tilted from the normal direction (in the case of gliding) [Figs. 12(a) and 12(b)]. In order to perform the experiment in a controlled way one should first prepare the system in the state with the

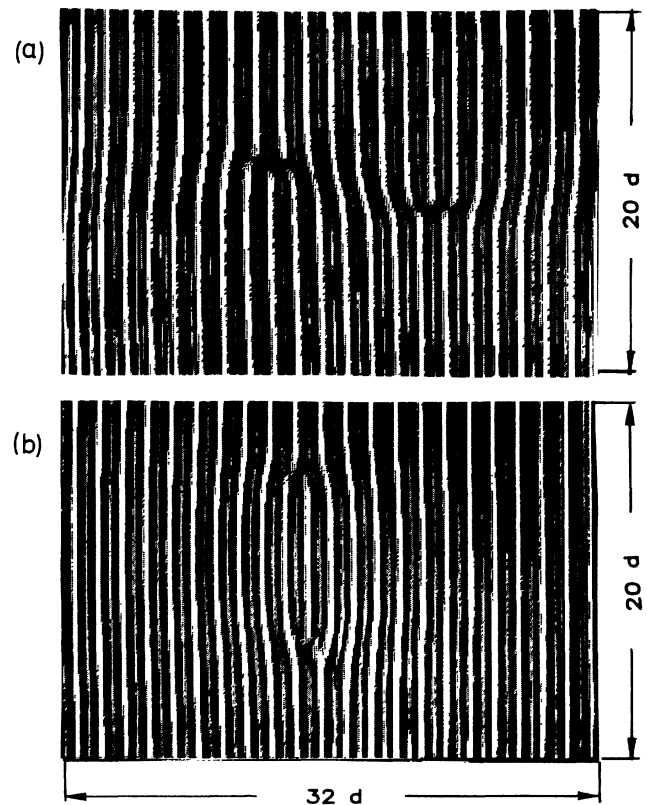


FIG. 12. Shadowgraph pictures of Williams rolls with two annihilating defects of opposite topological charge: (a) glide and (b) climb.

chosen  $k$ . Then in order to create defects one needs to adjust the control parameter  $\epsilon$  above the value for a defect creation which in our cell happens to be at  $\epsilon=0.08$ . After some defects were created the voltage was switched back to a value of  $\epsilon$  at which the defect motion is supposed to be investigated. After a while most of the defects are annihilated until a few defects remain in the whole cell (about 1 defect on several hundred rolls). Then the velocity of an isolated defect and the wave number of the underlying pattern are measured.

To perform this experiment we used several experimental techniques. First, to produce a pattern with the chosen wave number we used the frequency dependence of the wave number of the WR [Fig. 1(b)]. The experimental procedure was the following. The state with only a few defects was reached at a frequency different from the working frequency with a  $k$  different from  $k_c$  at the working frequency. Then the frequency and the amplitude of the external driving voltage were rapidly adjusted to the working frequency ( $f/f_c=0.2$  in our experiment) and the chosen value of the control parameter  $\epsilon$ . Due to this rapid change the optimal wave number  $k_f(f)$  changes, and this results in a wave-number difference  $\Delta k = k - k_f$  because the wave number  $k$  of the pattern will not change with this jump, as long as it is inside the stable band. In this way it was possible to scan the whole band of stable wave numbers for the WR. The reason for choosing the mentioned value for  $f/f_c=0.2$  was to reach the whole band of stable wave numbers by the frequency variation.

Using these techniques we measured the velocity of a single defect as a function of the wave-number difference  $\Delta k$ . The results of these measurements for two values of the control parameter  $\epsilon=0.03$  (squares) and  $\epsilon=0.06$  (triangles) are shown in Fig. 13. The solid line is a linear fit to the data. The dashed line is the theoretical prediction from Fig. 23 which will be described in Sec. V. Each point on the graph was obtained by taking ten pictures of the moving defect at fixed time intervals. Using the digital filtering technique described in Sec. II, we pinpointed

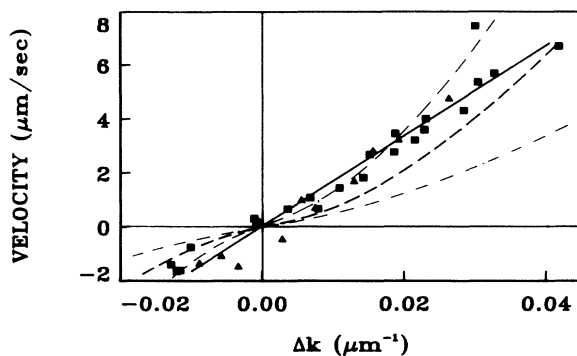


FIG. 13. Constant defect velocity as a function of the wave-number difference between  $k$  and  $k_f$ . The solid line is a linear fit to the data. Triangles and squares present measurements at  $\epsilon=0.03$  and  $0.06$ , respectively. The dashed line is a theoretical prediction of Ref. 23, the dash-dotted lines indicate the range of this prediction due to the experimental errors for  $\xi_{||}^0$ ,  $\xi_{\perp}^0$ , and  $\tau_0$ .

the defect location at the crossing point of the lines  $\text{Re}(A)=0$  and  $\text{Im}(A)=0$  [see Fig. 2(b)]. An example of a measurement of the velocity of a single defect is given in Fig. 14. With this technique we are able to reach an accuracy in the velocity measurement better than 1%.

The existence of a uniform defect velocity in a nonequilibrium structure has already been observed.<sup>4,21</sup> However, it was only observed in the range where the control parameter is far outside of the validity domain of perturbative theories. Moreover, as was already pointed out, at values of  $\epsilon$  closer to the convection onset this behavior was not observed and the defect velocity did not reach zero at the wave number  $k=k_f$  in the experiment described in Ref. 21. This could be because of the experimental techniques which were used there.<sup>31</sup> This defect dynamics leads to the wave-number selection predicted theoretically,<sup>24,25</sup> while the experiment in an isotropic flow<sup>4</sup> did not present the evidence of this selection at low values of the control parameter  $\epsilon$  ( $\epsilon \ll 1$ ). The essential difference demonstrated by our results with those obtained in the Rayleigh-Bénard convection is the existence of the uniform velocity of the defect motion to zero values of  $\Delta k$  at  $\epsilon$  as small as  $10^{-3}$ . This is an experimental verification of the selection mechanism due to the defect climbing suggested for an isotropic<sup>7-9</sup> as well as an anisotropic<sup>23,24</sup> fluid. The theory suggests that the uniform defect velocity is the result of a balance between elastic force and dissipation. The elastic force which acts on a dislocation is similar to the Peach-Koehler force acting on a dislocation in a crystal under the stress caused by interaction of a strain produced by a dislocation and external stress.<sup>7-9</sup> Due to this analogy the external stress exerted on the nonequilibrium structure is the wave-number difference  $\Delta k$ . Therefore the defect climbing may occur in both directions along the roll axis depending on the sign of  $\Delta k$ . Thus for  $\Delta k > 0$  where the pattern is narrower with respect to the optimal one, the dislocation with an additional pair of rolls will climb downward in order to insert one pair of rolls, and an opposite motion will occur for  $\Delta k < 0$ . That is exactly what was observed in the experiment and is presented in Fig. 13.

Using the same procedure and experimental technique we followed also the dynamics of two defects on their way to pairwise annihilation. Since defects always are

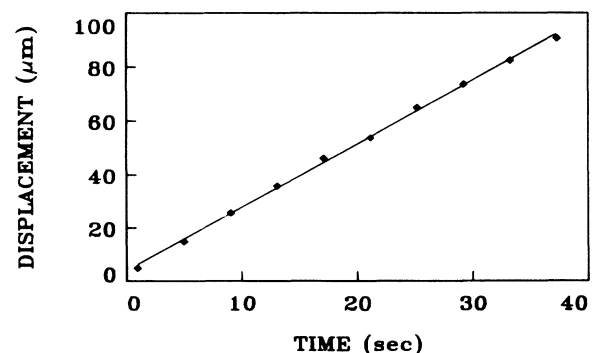


FIG. 14. Distance vs time for a single-defect motion.  $\epsilon=0.02$ ,  $\Delta k=0.008 \mu\text{m}^{-1}$ ,  $u=1.6 \mu\text{m}/\text{sec}$ .

nucleated in pairs one can find a couple of defects at a large enough distance apart, moving toward each other and far away from other defects (about 100 rolls). In this case, two defects move first with a constant velocity toward each other if the wave-number difference of the underlying pattern is different from zero and the pattern prefers to expel a pair of the rolls. At a later stage when the defects in the pair come closer they are accelerated due to the attraction. In a climbing motion two defects move along the roll axis as shown in Fig. 12(b). An example of this behavior is shown in Fig. 15(a) where the distance of the defects in dependence on the time is plotted.

We observed both climb and glide in the experiments. While climbing is smooth, a defect motion which consists predominantly of gliding [Fig. 12(a)] shows steplike behavior [Fig. 15(b)]. This modulation of the velocity with a periodicity given by the roll pattern is the result of the so-called “nonadiabatic effects” which couple the slow and the fast variables.<sup>32</sup> The existence of the pinning effect in a glide motion was predicted first in Ref. 9 for an isotropic flow and then in Ref. 23 for an anisotropic flow.

It was found experimentally that the distance where the peach-Koehler force comes in the range of the size of the attractive force is proportional to the inverse wave-number difference  $1/\Delta k$  (Fig. 16). At small values of  $\Delta k$  it reaches a value of at least one magnitude larger than the coherence length in the system.

On the basis of the experimental observations the following essential features of the defect motion should be noticed.

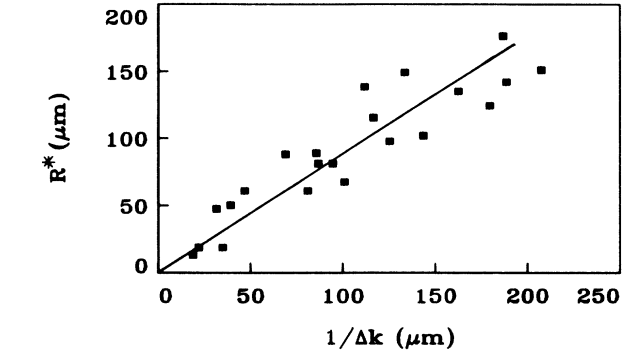


FIG. 16. The crossover distance  $R^*$  as a function of  $1/\Delta k$ .  $R^*$  was measured by taking the intersection of a linear fit to the upper part of measurements of the kind presented in Fig. 15(a), and a quadratic fit to the lower part.  $R^*$  presents the distance where the attraction force becomes dominant.

(i) For a distance between the dislocations being large enough there exists a regime with a uniform relative velocity of the defects.

(ii) Two kinds of forces acting on defects were observed: One which caused the defect motion at the constant velocity in the direction perpendicular to  $\Delta k$  is an analog to the Peach-Koehler force exerted on dislocations in crystals; and the other one is an attractive force which is acting between a pair of defects and causes their acceleration toward annihilation. The distance  $R^*$ , where the attractive force becomes visible, is for small  $\Delta k$  much larger than the coherence length.

## V. DISCUSSION OF THE RESULTS AND COMPARISON WITH THE THEORIES

There are two theories<sup>23,25</sup> of defect dynamics in EHC at the moment which can be compared with the experimental results presented above. One theory<sup>23</sup> which is basically similar to the theory of defect dynamics in an isotropic fluid is based on the GL equation. The main assumption of this theory is that the structure, dynamics, and nucleation of topological defects can be described by the GL equation. According to the theory stationary dislocations exist only at  $\Delta k=0$ . For  $\Delta k \neq 0$  the direction of motion is perpendicular to  $\Delta k$  and can, therefore, take on any direction (climb or glide) which is very different from the isotropic case where glide occurs only in a nonpotential situation. The relation between the velocity and the wave-number mismatch for  $|\mathbf{U}|=U \ll 1$  is predicted<sup>23</sup> to be

$$U \ln(3.29/U) = -2\Delta q \quad \text{for } UR \gg 1, \quad (5a)$$

$$U \ln(R/1.13) = -2\Delta q \quad \text{for } UR \ll 1, \quad (5b)$$

where  $\mathbf{U}=(U_x, U_y)$ ,  $\Delta \mathbf{q}=(\Delta q_x, \Delta q_y)$  are the velocity and the wave number in scaled units:

$$U_x = u_x(\tau_0/\xi_{\parallel}^0)\epsilon^{-1/2}, \quad U_y = u_y(\tau_0/\xi_{\perp}^0)\epsilon^{-1/2},$$

$$\Delta q_x = \Delta k_x \xi_{\parallel}^0 \epsilon^{-1/2}, \quad \Delta q_y = \Delta k_y \xi_{\perp}^0 \epsilon^{-1/2},$$

and  $R=(r/\xi_{\parallel}^0)\epsilon^{1/2}[1+(\xi_{\parallel}^0/\xi_{\perp}^0)^2]^{1/2}$  is the horizontal size of the system in scaled units.

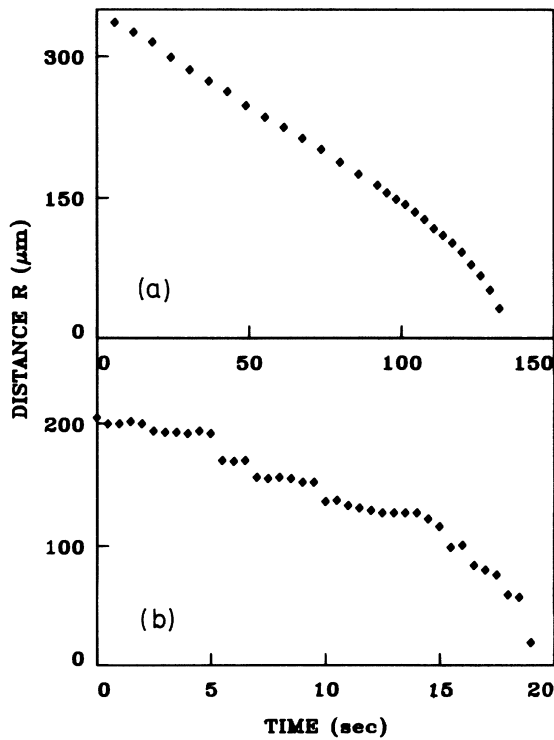


FIG. 15. Distances between two topological defects on their way to annihilation as a function of time. (a) The motion is predominantly climb. (b) The motion is predominantly glide.

Equations (5a) and (5b) are analytic approximations valid for a range of  $\Delta k$  up to  $0.02 \mu\text{m}^{-1}$ . For larger  $\Delta k$  full numerical calculations are necessary. The result of these calculations<sup>33</sup> is given in Fig. 13 for the limiting case  $UR \gg 1$ , which corresponds to our experimental data. The dashed line is this result for  $\epsilon=0.06$  using the experimental values  $\tau_0=0.048$  sec,  $\xi_1^0/d=0.12$ , and  $\xi_{\parallel}^0/d=0.26$ . The dash-dotted lines indicate the range of this solution due to the experimental errors for  $\tau_0$ ,  $\xi_{\parallel}$ , and  $\xi_1$ . The dynamics of defect pairs was also discussed within the framework of this theory.<sup>23</sup> A comparison of these theoretical results with two sets of experimental data with mostly climb motion are given in Fig. 17 (solid lines). The coefficients of the GL equation and  $\Delta k_x$  for the theoretical calculations were taken from the experiment. It is also possible to explain the linear dependence of the crossover distance  $R^*$  on  $1/\Delta K$  (Fig. 16) within the framework of the GL equation<sup>23</sup> or the phase diffusion equation<sup>15,16</sup> by noting that the distortion in front of a moving defect is screened over a distance  $\xi^2 U / \tau_0 \propto 1/\Delta q$ .

Another theory<sup>25</sup> is based on a different approach. The authors of Ref. 25 claim that singularities in the order-parameter field cannot be described by the GL equation, because the GL equation describes only long-wavelength perturbations of the amplitude and therefore cannot describe the defect core when the amplitude becomes zero. The presence of topological defects suggests the introduc-

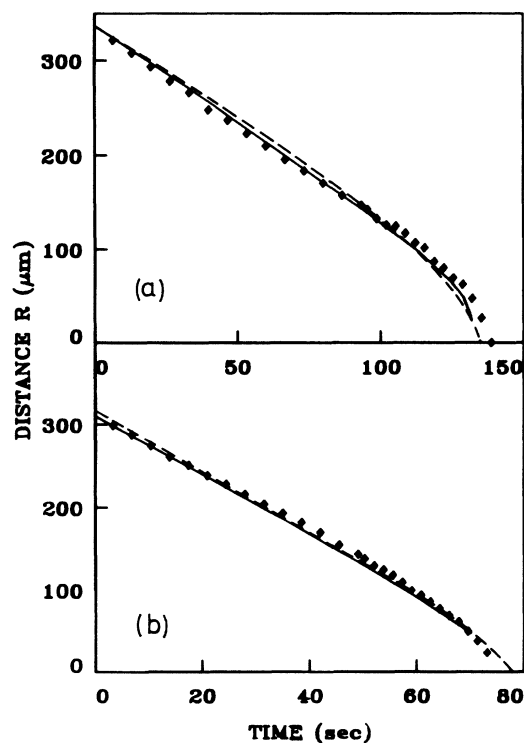


FIG. 17. Distance between two topological defects on their way to annihilation as a function of time. The data pertain to  $\epsilon$  values of (a) 0.033 and (b) 0.06 and  $\Delta k$  values of (a)  $0.0064 \mu\text{m}^{-1}$  and (b)  $0.01 \mu\text{m}^{-1}$ . The solid lines are the prediction from the theory of Ref. 23 and the dashed lines are the prediction from the theory of Ref. 25.

tion of an additional field which, from symmetry considerations, can be presented by a gauge field. A description based on the GL equation coupled with the gauge field equation was suggested to understand the interaction of defects. In Ref. 3 we have already made a detailed comparison of our data with this theory. Here we would like to outline the main results. The theory<sup>25</sup> predicts a linear dependence of the defect velocity (an isolated defect or two defects far away from each other) on the wave-number difference  $\Delta k$  and independence on the control parameter  $\epsilon$ . From the slope of the linear fit in Fig. 13 the coupling constant between the gauge and the order-parameter field can be found. This coupling constant defines in its turn the second characteristic length of the theory, the penetration length  $\lambda$  which from our data happens to be about  $\lambda \cong 21\xi$ . Then the theory allows the relative distance between two defects to be calculated as a function of time. The dash-dotted lines in Figs. 17(a) and 17(b) present examples for the theoretical calculations for defect annihilations (the parameters  $\tau_0$ ,  $\xi_{\parallel}$ ,  $\xi_1$ ,  $\Delta k_x$  needed for the calculations were taken from the experiment). Also the linear dependence of  $R^*$  on  $1/\Delta k$  can be explained with this theory which predicts the attraction distance for two defects to be proportional to  $1/\Delta k$ .

In conclusion, on the current stage of the experiment we are not able to choose between the two theories in spite of significant differences in their basic assumptions. Both theories are able to explain the linear dependence of  $R^*$  on  $1/\Delta k$  and also the path of annihilation for two defects. The dependence of the velocity of a single defect on  $\Delta k$  can also be explained by both theories but, of course, in the theory of Ref. 25 there exists one fit parameter which still has to be calculated from the basic equations. More experiments, made in a range where the theories yield different predictions, are required to check the validity of them. One example for such an experiment could be the measurement of the defect velocity in dependence on the aspect ratio of the sample. For  $UR \ll 1$  the theory of Ref. 23 [Eq. 5(b)] predicts a size dependence of the defect motion, while the theory of Ref. 25 does not (as long as the size of the sample is large compared to  $\lambda$ ). Another possibility to decide experimentally between the two theories could be a check of the dependence of the defect motion on the control parameter  $\epsilon$ . For Ref. 25 there is none and for Ref. 23 it depends on  $\epsilon^{1/2}$ . In our experiment the scatter of the data in Fig. 13 is too large to decide about the  $\epsilon$  dependence. One possibility to reduce this scatter would be to perform similar experiments for a larger range of the control parameter. For large values of the control parameter  $\epsilon$ , however, the two theories would leave their range of validity.

#### ACKNOWLEDGMENTS

We would like to thank G. Goren, I. Procaccia, L. Kramer, and E. Bodenschatz for discussions, valuable comments, and suggestions. This work was supported in part by the Minerva Foundation, Heidelberg, W. Germany, and U.S.-Israel Binational Science Foundation. I.R. and S.R. would also like to thank the Deutsche Forschungsgemeinschaft (DFG) for financial support.

- <sup>1</sup>J. P. Gollub and J. K. Steinmann, *Phys. Rev. Lett.* **47**, 505 (1981); G. Ahlers, D. S. Cannel, and V. Steinberg, *Phys. Rev. Lett.* **54**, 1373 (1985); A. Pocheau, V. Croquette, and P. Lega, *Phys. Rev. Lett.* **55**, 1099 (1985).
- <sup>2</sup>X. D. Young, A. Joets, and R. Ribotta, in *Propagation in Systems Far from Equilibrium*, edited by J. E. Wesfreid, H. R. Brand, P. Manneville, G. Albinet, and N. Boccara (Springer, Berlin, 1987), p. 194.
- <sup>3</sup>G. Goren, I. Procaccia, S. Rasenat, and V. Steinberg, *Phys. Rev. Lett.* **63**, 1237 (1989).
- <sup>4</sup>A. Pocheau and V. Croquette, *J. Phys. (Paris)* **45**, 35 (1984).
- <sup>5</sup>A. Joets and R. Ribotta, *J. Phys. (Paris)* **47**, 595 (1986).
- <sup>6</sup>J. A. Whitehead, *J. Fluid Mech.* **75**, 715 (1976).
- <sup>7</sup>E. D. Siggia and A. Zippelius, *Phys. Rev. A* **24**, 1036 (1981).
- <sup>8</sup>Y. Pomeau, S. Zaleski, and P. Manneville, *Phys. Rev. A* **27**, 2710 (1985).
- <sup>9</sup>G. Tesauro and M. C. Cross, *Phys. Rev. A* **34**, 1363 (1986).
- <sup>10</sup>E. D. Siggia and A. Zippelius, *Phys. Fluids* **26**, 2905 (1983).
- <sup>11</sup>E. D. Siggia and Z. Zippelius, *Phys. Rev. Lett.* **47**, 835 (1981).
- <sup>12</sup>P. Couillet, C. Elphick, L. Gil, and J. Lega, *Phys. Rev. Lett.* **59**, 884 (1987).
- <sup>13</sup>E. Guazzelli, E. Guyon, and J. E. Wesfreid, in *Symmetries and Broken Symmetries in Condensed Matter Physics*, edited by N. Boccara (IDSET, Paris, 1981), p. 455.
- <sup>14</sup>E. Guazzelli, E. Guyon, and J. E. Wesfreid, *Philos. Mag. A* **48**, 709 (1983).
- <sup>15</sup>E. Dubois-Violette, E. Guazzelli, and J. Prost, *Philos. Mag. A* **48**, 72 (1985).
- <sup>16</sup>J. Prost, E. Dubois-Violette, E. Guazzelli, and M. Clement, in *Cellular Structures in Instabilities*, edited by J. E. Wesfreid and S. Zaleski (Springer, Berlin, 1984).
- <sup>17</sup>I. Rehberg, S. Rasenat, and V. Steinberg, *Phys. Rev. Lett.* **62**, 756 (1989).
- <sup>18</sup>H. Yamazaki, S. Kai, and K. Hirakawa, *J. Phys. Soc. Jpn.* **56**, 1 (1987).
- <sup>19</sup>S. Kai, in *Noise in Nonlinear Dynamical Systems*, edited by F. Moss and P. V. E. McClintock (Cambridge University Press, Cambridge, 1988), Vol. 3, Chap. 2.
- <sup>20</sup>S. Kai, N. Chizumi, and M. Kohono, *J. Phys. Soc. Jpn.* **58**, 1493 (1989).
- <sup>21</sup>S. Nasumo, S. Takeuchi, and Y. Sawada, *Phys. Rev. A* **40**, 3457 (1989).
- <sup>22</sup>M. Sano, S. Nasumo, and Y. Sawada (unpublished).
- <sup>23</sup>E. Bodenschatz, W. Pesch, and L. Kramer, *Physica D* **32**, 135 (1988).
- <sup>24</sup>L. Kramer, E. Bodenschatz, W. Pesch, W. Thom, and W. Zimmermann, *Liq. Cryst.* **5**, 699 (1989).
- <sup>25</sup>G. Goren and I. Procaccia (unpublished).
- <sup>26</sup>J. Wesfreid, Y. Pomeau, M. Dubois, C. Normand, P. Berge, *J. Phys. (Paris)* **39**, 75 (1978).
- <sup>27</sup>See, e.g., E. Bodenschatz, W. Zimmermann and L. Kramer, *J. Phys. (Paris)* **49**, 1875 (1988), and references therein.
- <sup>28</sup>W. J. A. Goozens, *Ad. Liq. Cryst.* **3**, 1 (1978), and references therein.
- <sup>29</sup>S. Rasenat, G. Hartung, B. Winkler, and I. Rehberg, *Exp. Fluids* **7**, 412 (1989).
- <sup>30</sup>We are thankful to E. Bodenschatz for the suggestion.
- <sup>31</sup>In the recently published paper (Ref. 21) a similar result was obtained in anisotropic flow. The authors were aware that their result contradicts the theory, and argue that it is due to the experimental techniques used. Moreover, contrary to what we present here and in Ref. 3, the authors of Ref. 21 came to the conclusion that the characteristic length of defect interaction is on the order of the pattern wavelength.
- <sup>32</sup>Y. Pomeau, *Physica D* **23**, 3 (1986).
- <sup>33</sup>L. Kramer, E. Bodenschatz, and W. Pesch (unpublished).

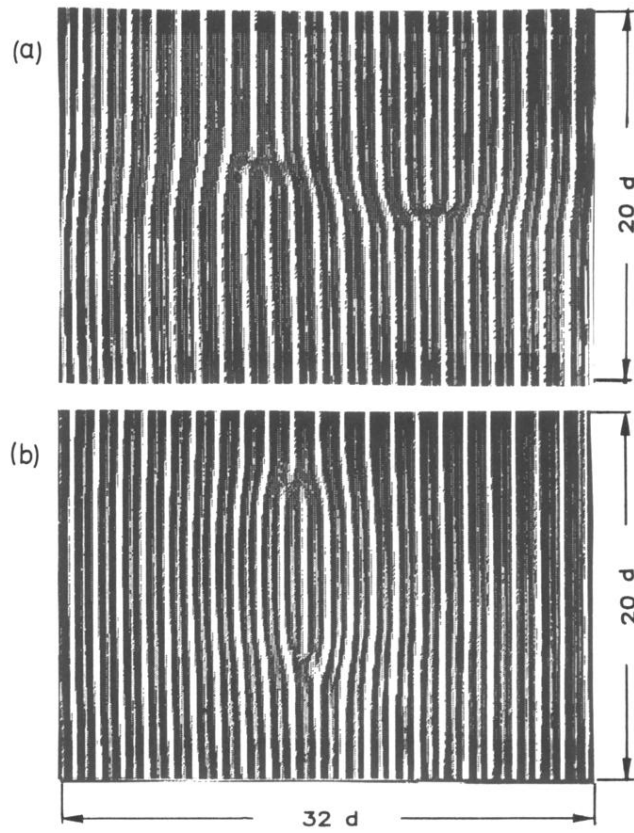


FIG. 12. Shadowgraph pictures of Williams rolls with two annihilating defects of opposite topological charge: (a) glide and (b) climb.

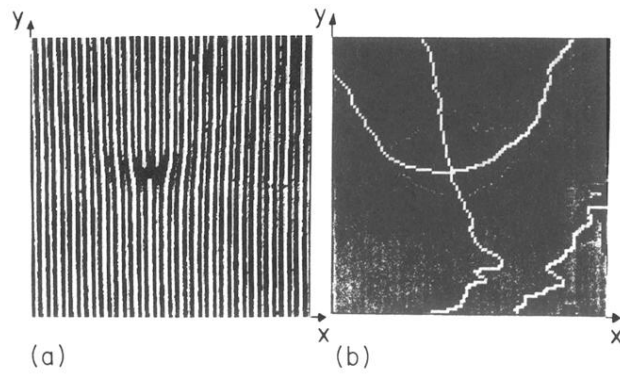


FIG. 2. (a) A shadowgraph image of a single defect in Williams rolls, and (b) the corresponding field of the absolute value of the amplitude and two lines corresponding to  $\text{Re}(A)=0$  and  $\text{Im}(A)=0$ .

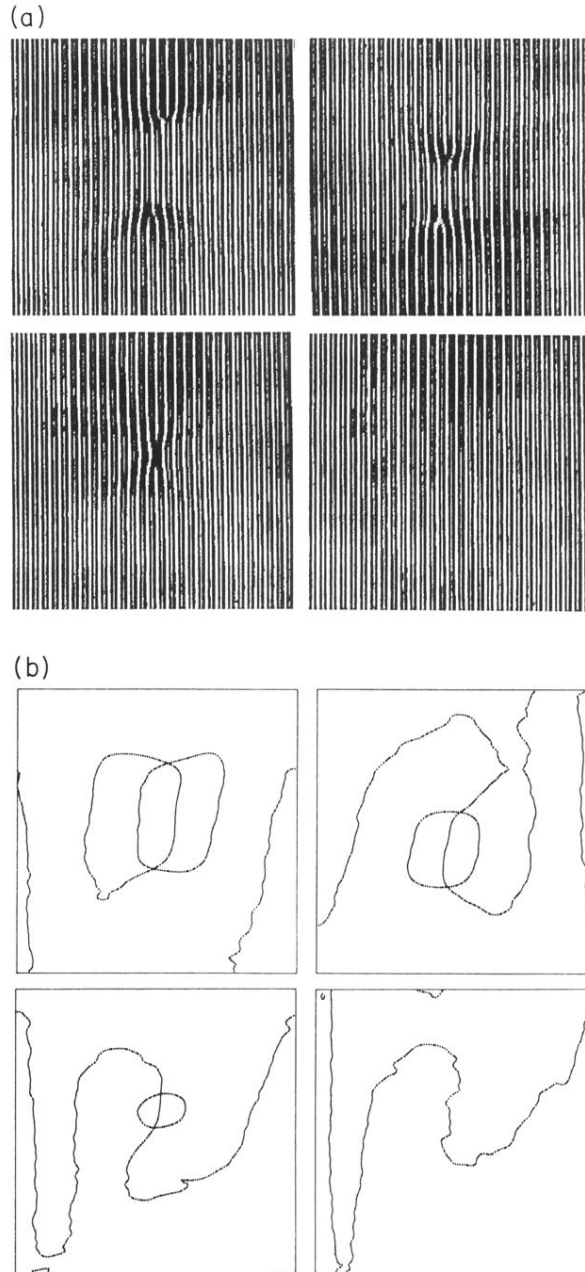


FIG. 3. (a) Dynamics of defect annihilation presented in four pictures in time, and (b) the same process but presented in the phase field plane after the digital filtering.